ADVANCED QUANTUM TECHNOLOGIES
www.advquantumtech.com

Strain-Free GaSb Quantum Dots as Single-Photon Sources in the Telecom S-Band

Johannes Michl, Giora Peniakov, Andreas Pfenning, Joonas Hilska, Abhiroop Chellu, Andreas Bader, Mircea Guina, Sven Höfling, Teemu Hakkarainen, and Tobias Huber-Loyola**

Generating single photons in the telecommunication wavelength range from semiconductor quantum dots (QDs) and interfacing them with spins of electrons or holes is of high interest in recent years, with research mainly focusing on indium-based QDs. However, there is not much data on the optical and spin properties of gallium antimonide (GaSb) QDs, despite it being a physically rich system with an indirect to direct bandgap crossover in the telecom wavelength range. This work investigates the (quantum-) optical properties of GaSb QDs, which are fabricated by filling droplet-etched nanoholes in an aluminum gallium antimonide (AlGaSb) matrix. Photoluminescence (PL) features from isolated and highly symmetric QDs are observed that exhibit narrow linewidth in the telecom S-band and show an excitonic fine structure splitting of up to $\Delta E_{FSS} = (12.0 \pm 0.5)$ μeV. Moreover, time-resolved measurements of the decay characteristics of an exciton are performed and the second-order photon autocorrelation function of the charge complex is measured to $g^2(0) = 0.16 \pm 0.02$, revealing clear antibunching and thus proving the capability of this material platform to generate non-classical light.

1. Introduction

Non-classical light sources are a major building block in quantum communication applications as well as for photonic quantum computing.[1] Compared to several other physical systems like vacancy centers in diamond[2] and trapped atoms,[3] which can provide single photons, semiconductor quantum dots (QDs) offer superior optical properties like low multi-photon contribution[4–6] and high indistinguishability.[7–10]

Protocols for secure long-range communication like quantum key distribution (QKD)[11] call for the exploitation of existing fiber networks, or costly satellite.[12] Emission wavelengths in the telecommunication spectral window are of particular interest since they offer the least absorption and wave packet dispersion of photons in optical fibers. The experimental implementation of QKD protocols has succeeded in over several hundred kilometers of optical fiber using modulated laser pulses.[13] However, the usage of weak laser pulses introduces multi-photon events offering possibilities for eavesdropping, which must be mitigated by more complicated protocols. Furthermore, weak coherent pulses are fundamentally limited in photon indistinguishability due to their Poisson statistic and therefore outperformed by single photon sources like QDs in most QKD applications as soon as interference is required.[14]

In the near infrared (NIR) regime, gallium arsenide (GaAs) QDs have shown to be a source of highly indistinguishable photons with near-unity visibility.[15] These photons were used in the telecom range to demonstrate two-photon interference from few kilometers[16] to over 300 km of optical fiber using frequency conversion techniques.[17] Furthermore, for photons generated directly in the telecom C-band quantum teleportation and interference of a single photon with a laser qubit has also been demonstrated recently.[18]

This shows that QDs in various material platforms can provide highly indistinguishable single photons in the telecom range to scale future experiments to measurement device independent quantum key distribution (MDI-QKD)[19] and to extend to quantum repeaters.[20] Over the last few years, several QD

J. Michl, G. Peniakov, A. Pfenning, A. Bader, S. Höfling, T. Huber-Loyola
Julius-Maximilians-Universität Würzburg
Physikalisches Institut
Lehrstuhl für Technische Physik
Am Hubland
Würzburg 97074, Deutschland
E-mail: johannes.michl@physik.uni-wuerzburg.de;
tobias.huber@physik.uni-wuerzburg.de

J. Hilska, A. Chellu, M. Guina, T. Hakkarainen
Optoelectronics Research Centre
Physics Unit / Photonics
Faculty of Engineering and Natural Sciences
Tampere University
Tampere 33014, Finland

The ORCID identification number(s) for the author(s) of this article can be found under https://doi.org/10.1002/qute.202300180

DOI: 10.1002/qute.202300180

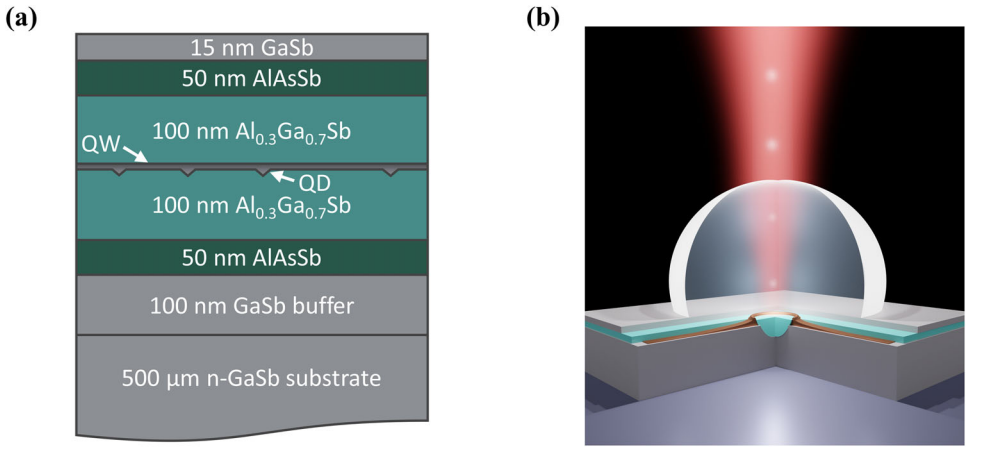

Figure 1. Sample design and layer structure. a) Detailed schematic of the layer sequence. A GaSb substrate and buffer is used, followed by 50 nm of AlAsSb. The droplets are etching holes into a 100 nm layer of $Al_{0.3}Ga_{0.7}Sb$ which are then filled with GaSb, followed by an $Al_{0.3}Ga_{0.7}Sb$ layer of identical thickness as the first. The layer structure ends with 50 nm of AlAsSb and a 15 nm GaSb cap. b) Simplified, artistic view of the sample, including the filled nanohole forming a QD, surrounded by the quantum well (QW) area. A solid immersion lens is placed over the whole sample, increasing the collection efficiency of the emitted photons (depicted as bright light bundles). The laser is drawn as a red, Gaussian shaped beam.

material platforms like indium (gallium) arsenide (In(Ga)As)/GaAs and indium arsenide (InAs)/indium phosphide (InP)[21] have emerged as resources for non-classical light in the wavelength range ≈1550 nm.[22] In particular, the use of a metamorphic buffer (MMB) layer was utilized to shift the emission of InAs QDs into the telecom range[23] creating single photons[24,25] and polarization-entanglement.[26] First attempts to increase collection efficiency in free space[27,28] as well as fiber-coupled by integrating telecom InAs QDs into photonic structures[29] have been demonstrated, and first steps into plug and play devices for quantum key distribution (QKD) in the telecom O-band have been realized.[30]

While all these approaches cover the need for low losses on the photonic side, the other pressing requirement for memory-based quantum repeaters is control over the matter qubit, which in the case of QDs is the electron or hole spin. In previous works on InAs/GaAs QDs, we have shown the demonstration of full coherent control of a spin-qubit emitting in the telecom C-band.[31] However, the spin coherence times were very short ($T_2^* = 240$ ps[31]), limiting the usability of the system when approaching implementation of the QDs in quantum repeater applications. The times to which the coherence of an optically active spin-qubit can be extended (e.g. through dynamical decoupling techniques) are, amongst others, governed by the nuclear spins.[32] In this indium plays a dominant role as was experimentally shown in recent years,[33] as it has a large nuclear spin of $s_{N,In} = \frac{9}{2}$ (In comparison: $s_{N,As} = \frac{3}{2}$, $s_{N,Ga} = \frac{3}{2}$, $s_{N,Sb} = \frac{5}{2}$). An example of an indium-free material platform is GaAs QDs, grown by droplet etching epitaxy on aluminum gallium arsenide (AlGaAs), which has been shown to be a source of non-classical light of high quality[34] in the wavelength range of 780 nm. Using GaAs QDs and exploiting decoupling techniques, recent work could extend electron spin coherence times into the millisecond range.[35] Indium-free QDs are thus very promising to extend the coherence times of semiconductor QDs, but the GaAs material system is limited to the short wavelength range. GaSb QDs are a promising indium-free QD candidate to make comparably long coherence times also available in the telecom wavelength range.

In this work, we investigate the unexplored quantum-optical properties of GaSb QDs, grown by local droplet etching of nanoholes and subsequent filling. We show first results of time-resolved as well as autocorrelation measurements of emission features from single GaSb QDs emitting in the telecom S-band. Our results pave the way to exploit this material platform, which combines the low losses of photons in the telecom range with possibly long spin coherence times due to the lack of indium.

2. Sample Design and Heterostructure Growth

The GaSb QDs investigated in this study were grown by solid-source molecular beam epitaxy (MBE) on GaSb(100) substrates by GaSb filling of nanoholes etched into AlGaSb via local droplet etching.[36] This method was first developed for the GaAs/AlGaAs system[37,38] and has been recently extended to the GaSb/AlGaSb system (see previously published articles,[39,40] including more details on the growth of our sample).

The exact heterostructure is provided in **Figure 1**a. After oxide desorption, the growth process is started by depositing a 100 nm thick GaSb buffer followed by 50 nm of aluminum arsenide antimonide (AlAsSb) and 100 nm of aluminum gallium antimonide ($Al_{0.3}Ga_{0.7}Sb$). The local droplet etching is initiated by depositing 1.5 monolayers (MLs) of Al with a 0.3 ML s^{-1} flux at a temperature 395 °C under a low Sb-flux of 0.07 ML s^{-1}. The excess Al forms a uniform distribution of metal droplets on the surface with a density of 2.6×10^7 cm^{-2}, which then etch into the underlying $Al_{0.3}Ga_{0.7}Sb$ matrix forming ≈ 12 nm deep nanoholes.[40] The nanoholes are subsequently filled by GaSb and then encapsulated by $Al_{0.3}Ga_{0.7}Sb$. In this study, a thickness of the GaSb-filling layer of 20 ML was used. To promote carrier capture into the QDs, the $Al_{0.3}Ga_{0.7}Sb$ /GaSb-QD/ $Al_{0.3}Ga_{0.7}Sb$ structure was encased within $AlAs_{0.08}Sb_{0.92}$. The topmost $AlAs_{0.08}Sb_{0.92}$ is protected from atmospheric oxidation by a thin 15 nm GaSb capping

layer. For more efficient collection of the emitted PL, a solid immersion lens (SIL) was placed over the whole sample, as can be seen in the artistic drawing of our sample in Figure 1b.

3. Experimental Data and Discussion

3.1. Setup and Methods

The sample was mounted in a closed-cycle cryostat, which allows for keeping a stable position for up to several weeks while keeping the sample at a base temperature of T = 1.57 K. For excitation, a fiber-coupled continuous-wave laser with a wavelength of 940 nm was used (further called cw-laser) as well as a ps-pulsed optical parametric oscillator (OPO) with identical wavelength as the cw-laser and a repetition rate of 80 MHz (further called pulsed laser).

In the detection path, polarization optics (quarter-wave plate, half-wave plate, and linear polarizer, further called QWP, HWP, and LP) were installed, to perform polarization-resolved PL-measurements. The QD signal was then fiber coupled and analyzed in a 750 mm Czerny-Turner spectrometer for its spectral components and detected with an indiumgalliumarsenide (InGaAs)-camera. A fiber-coupled variable bandpass filter was used to isolate single emission lines from individual charge complexes for further analysis. To resolve the signal temporally, the filtered signal was redirected onto superconducting nanowire single photon detectors (SNSPDs), connected to correlation electronics, which can be triggered by the laser.

3.2. μ-PL Spectra and Characterization

The fundamental optical properties of individual GaSb QDs are studied by means of micro photoluminescence (μ-PL). The average QD density of 2.6×10^7 cm^{-2} ensures that individual QDs can be addressed and excited. In agreement with earlier reports,[40] we could observe PL-emission in the telecom S-band at ≈1470 nm.

Figure 2a depicts a spectrum that was obtained by exciting the QD with a wavelength of 940 nm, an excitation power of P = 1.89 μW and an integration time of 100 s. The most prominent emission feature (referred to as *main peak* from now on), is located at ≈ 1469.2 nm and highlighted by the red background in the spectrum. Surrounding it are various other discrete recombination features at higher wavelengths. These characteristics look similar to the PL from GaAs QDs, grown via droplet etching, under non-resonant excitation.[41] To analyze the underlying dynamics between the emission features and to identify the nature of the studied charge complex, we performed a power series. For this, we increased the laser pump-power from 0.27 to 3.84 μW and measured the PL emission spectra. Every such acquired spectrum was fitted with a Lorentzian multipeak fit to track the evolution of the peaks. The inset in the upper right corner of Figure 2a depicts the integrated intensity of the main peak, extracted from the fits, as a function of the excitation power on the double-logarithmic scale. A linear fit to the logarithmic axes yields a power-law coefficient of 1.03, pointing toward emission from a neutral exciton or a trion. For P > 2.5 μW, the main peak PL-intensity saturates.

Further information about the nature of the observed charge complexes was gathered by performing a polarization series. A structural asymmetry of the QD leads to a mixing of the spin states of the exciton and results in a fine-structure splitting (FSS),[42] while a trion on the other hand would not show any dependency on the polarization angle.[42] For this measurement, we placed a HWP in front of a LP in the detection path and rotated it from 0° to 180°, to measure the polarization-dependent spectra in all rectilinear projections. The normalized spectra are displayed in Figure 2b as a function of wavelength and HWP rotation angle in a colored contour plot. The main peak displays a subtle, visible oscillation with the rotation angle that can be further quantified by fitting the series, as is depicted in Figure 2c. A sinusoidal fit to the peak position versus the rotation angle yields a splitting amplitude of $\Delta\lambda_{FSS} = (0.021 \pm 0.001)$ nm corresponding to $\Delta E_{FSS} = (12.0 \pm 0.5)$ μeV, respectively. Together with the above analyzed power dependency of the peak intensity this suggests that the investigated charge complex is an exciton with a small FSS, which can be attributed to the slight asymmetry of the QDs. All the other emission lines in the shown spectrum show no polarization dependency. Furthermore, this is the largest FSS we found on this sample. This observation is in agreement with AFM and PL data from previous works[40] and strengthens our hypothesis that the measured QDs have low asymmetry.

3.3. Quantum-Optical Properties

To investigate the quantum-optical properties of the identified exciton, we performed a series of time-resolved measurements. We filtered the spectral line of the main peak using a variable bandpass filter and measured with a temporal resolution of about 20 ps using SNSPDs and correlation electronics.

3.3.1. Time Resolved Photoluminescence

By analyzing the temporal evolution of the PL-intensity measured on the SNSPDs, insight can be gained into the fundamental dynamics of charge carriers in our sample. For this, the pulsed laser was synchronizing the correlation electronics and set to an excitation wavelength of 940 nm. A pulse duration of ≈ 2 ps was used to excite the QD.

Figure 3a displays the time resolved PL data, with the spectrally resolved filtered main peak as an inset in the upper right corner. One can see clearly that there is a filling process of significant time.

Under above-bandgap excitation, multiple charge injection and decay channels are bound to contribute to the observed temporal signature, forming a complex system of coupled and time dependent populations. The details of the energy structure of the investigated GaSb QDs, including wavefunctions, effect of QD size on direct-indirect crossover, and allowed dipole transitions are reported in detail in another work of this group.[43]

To account for these charge carrier dynamics here, we assume the model that is illustrated in Figure 3b, where at a time t_0 after the laser pulse there are three reservoirs (QD, QW Γ-valley and QW L-valley) with three initial populations (x_0, G_0 and L_0) and time dependent evolutions ($X(t)$, $G(t)$ and $L(t)$), respectively. The proposed model includes the Γ and L-valley populations for the QW,[44] because at the given QW thickness the system is close

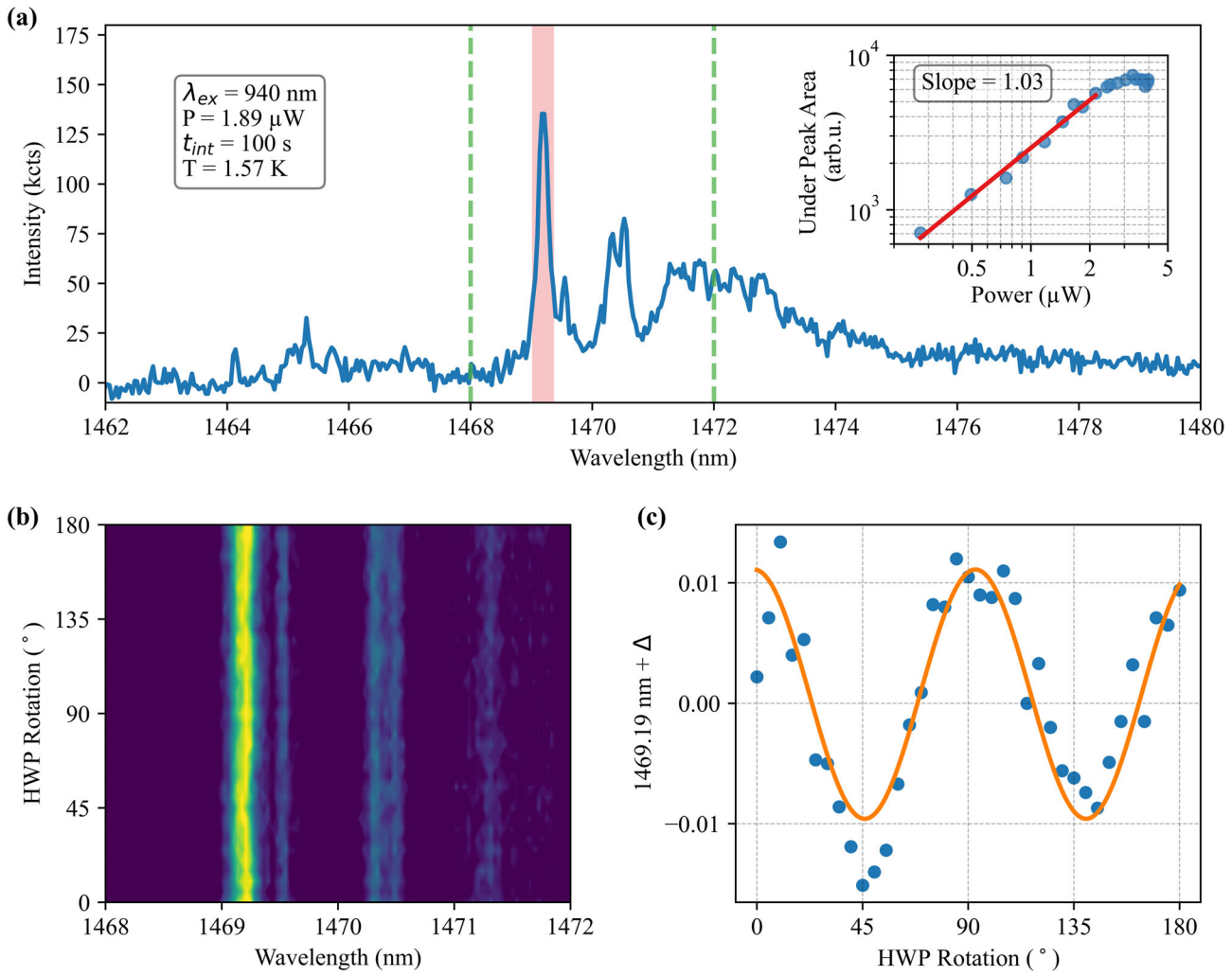

Figure 2. Micro photoluminescence for QD charge complex characterization. a) PL spectrum, acquired at T = 1.57 K with 100 s integration time under excitation with 940 nm. The brightest line is observed at ≈1469.2 nm (main peak) and highlighted with a red square background in the plot. The green dashed lines indicate the wavelength range resolved in (b). (Inset) Peak intensity of the main peak, vs. excitation power. Plotted on the double logarithmic scale, a power law coefficient of 1.03 can be derived from a linear fit function (solid red line). The PL intensity saturates for powers > 2.5 µW. b) False color plot of the normalized PL-spectra of a polarization series with the y-axis displaying the rotation of the HWP from 0° to 180°. A slight oscillation of the main peaks center wavelength position with the HWP rotation angle is visible, which is further quantified in (c). Here, the position of the main peak is extracted from a series of fits and plotted versus the HWP rotation. A sinusoidal fit to the data yields a fine structure splitting of $\Delta\lambda_{FSS}$ = (0.021 ± 0.001) nm or ΔE_{FSS} = (12.0 ± 0.5) µeV, respectively. The data displayed in this figure suggest, that the investigated charge complex is an exciton with small FSS.

to the Γ-L crossover point (cf. Figure S2, Supporting Information). Moreover, the L-valley of the QW has a higher density of states than the Γ-valley owing to the effective mass difference (applies also to the barrier), thus the L-valley population for the QW should be considered in case of above-bandgap excitation. The transition from L- to Γ-valley can take place by intervalley scattering.[45,46] Further details on the model are provided in the supplementary material. Equation (1) formulates the set of coupled differential equations which we use to describe the dynamics in this system:

$$\begin{cases} \dot{X}(t) = -a\,X(t) + b\,G(t) \\ \dot{G}(t) = -(b+c)\;G(t) + d\,L(t) \\ \dot{L}(t) = -d\,L(t) \end{cases}, \quad \begin{cases} X\;(0) = x_0 \\ G\;(0) = G_0 \\ L\;(0) = L_0 \end{cases} \tag{1}$$

The temporal evolution of the QD charge carrier population is governed by the decay rate "a" of excitons and the filling rate "b" from the QW Γ-valley. Meanwhile, the population in the Γ-valley is diminished through this decay to the QD, but also through radiative decay directly to the ground state with rate "c". The QW L-valley fills the Γ-valley with a rate "d". Here, the letters a–d correspond to the rates (i.)-(iv.) in Figure 3b.

Considering the above given rate equations, the experimentally acquired data can be described by the time dependent evolution $X(t)$. The set of differential equations is therefore solved (cf. supplementary material, Equation S1, Supporting Information) and fitted to the data as a solid red line in Figure 3a. Since our rate equation starts with a given filling at time zero and not with a temporal finite excitation pulse, an error function with width σ is multiplied to $X(t)$. Our true zero where the QD is

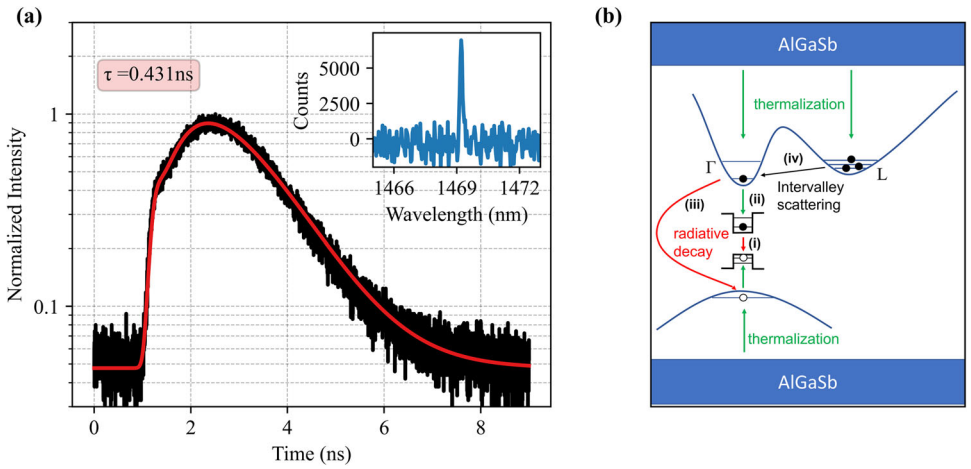

Figure 3. Temporal evolution of charge injection into and decay of excitons in the QD. a) Time resolved PL-intensity of the filtered emission line, which is displayed in the upper right inset (10 s integration time, on spectrometer). The red line is a fit to the data as detailed in the main text and yields a QD PL lifetime of $T_1^X = (431 \pm 10)$ ps. b) Theoretical model of the contributing processes. Rates, that must be considered for solving the differential equation describing the observed time trace, are: i) radiative decay of charge carriers in the QD excited state to the QD ground state, ii) filling of the QD through relaxation from the QW Γ-valley, iii) direct radiative decay from the QW Γ-valley to the ground state, and iv) scattering from the QW L-valley to the Γ-valley. Together with initial populations for QD, Γ-valley and L-valley, these rates form the system of coupled differential equations described in Equation (1).

filled and starts to decay is at about 1 ns in Figure 3a. From the fitted parameter a, the radiative lifetime $T_1^X = (431 \pm 10)$ ps can be inferred. A simple exponential fit, which would not follow our rate equation, would give a lifetime of (930 ± 9) ps, when fitting only times larger $t > 4$ ns.

From the rate equation, the decay time of the QW to the QD can be determined to 4.35 ns and is therefore the dominating process for the overall shape of the time trace. The slow trapping rate from QW to QD is consistent with the presence of an energy barrier of 5 meV observed for the GaSb QDs in temperature-dependent PL.[43] Additional data on the time-resolved PL characteristics of GaSb/AlGaSb QWs that support our model can be found in the supporting information (Figures S2–S5, Supporting Information).

Note that our model does not capture the underlying physics that are introduced by QD shape or strain that can be modeled by various methods.[47] It is rather a minimal phenomenological model, based on reasonable assumptions that can reproduce our data well. Band mixing of the QD states cannot be confirmed nor excluded from our data. However, even with mixed bands there is only a single ground state for the exciton. With mixing included, the indirect state of the GaSb QW is located in between Γ- and L-valley, but the physics would remain the same for the rate model.[48]

Our time resolved investigations of the excitonic emission line show that under above-bandgap excitation of a reservoir of charge carriers, the complex filling processes from the L- and Γ-valley of the QW to the QD play a predominant role. While these dynamics are of fundamental interest, they also show the need to excite the QDs resonantly in further experiments, as this will eliminate the filling through the QW. Under resonant pumping, an exponential fit of the time trace of the exciton would directly yield its radiative lifetime. Furthermore, resonant pumping could suppress the delayed re-excitation during one laser pulse from a reservoir, which strongly affects the single photon characteristics as we show in the following paragraph.

3.3.2. Second Order Autocorrelation Measurement

To evaluate how well single photons, originating from the discrete energy levels inside the QD, can be separated from any unwanted multiphoton background, we performed second order photon autocorrelation measurements. The same excitation conditions as for the measurement of the excitonic time trace were used. In this case, however, the signal was channeled through a 50:50 fiber beam-splitter onto two different channels of the single photon detectors that were connected to the correlation electronics. The correlation electronics were not synchronized to the laser any longer but operated in a "start/stop" manner, where one of the SNSPDs started the correlation measurement, while the other stopped it.

Figure 4 displays the autocorrelation measurement as a histogram of background corrected coincidences versus time delays Δt between detection events on the two detectors. The autocorrelation measurement, which is an approximation to the second order correlation function $g^{(2)}(\Delta t)$, shows a clear antibunching behavior of photons around zero time delay. To quantify the value of $g^{(2)}$ at zero time delay, the counts accumulated in the zero peak are normalized on the average of the accumulated counts in each side peak. The coincidence window, that is, the width of the integration, is set arbitrarily such that most of the counts are included, which in our case results in 8 ns. This yields a value $g^{(2)}_{\text{corrected}}(0) = 0.16 \pm 0.02$, which is about half the value from the raw data ($g^{(2)}_{\text{raw}}(0) = 0.32 \pm 0.01$). However, we want to describe the source as precisely as possible, and our detectors have a significant dark count rate compared to the rate of detected photons. Thus, we believe the background corrected value, where

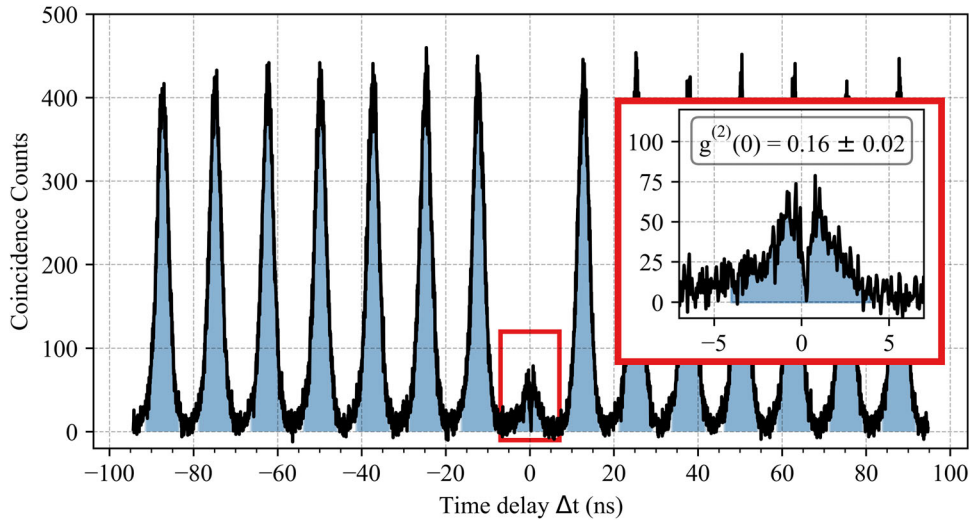

Figure 4. Autocorrelation measurement of the exciton recombination photons in Hanbury Brown-Twiss configuration. For zero time delay Δt, the number of measured coincidences is significantly lower than for non-zero delay times. Comparing the averaged integrated counts of peaks for t > 0 s with the peak at $t_0 = 0$ s using equal integration widths of 8 ns, one can derive a $g^2(0)$ value of 0.16 ± 0.02. Upper right inset: Magnified depiction of the observed dip in the central peak region, indicated by the red squares.

the background is calculated from independently measured dark-/ signal count rates reflects the source properties better. Details on the calculation of the background level as well as the data without background correction (Figure S1, Supporting Information) can be found in the supplemental information.

The inset in the upper right corner of Figure 4 zooms into the central peak, displaying an additional dip in the coincidence counts at Δt = 0 that reaches down near zero counts. We believe that the counts close to zero time delay accumulated in the central peak, which contribute mainly to the non-zero $g^2(0)$ value, are a direct result of the refilling from the QW, as explained in the lifetime measurement (see section 3.3.1). This leads to multiple excitations during one laser pulse. While this increases the number of photons contaminating the single-photon characteristics of our non-resonantly excited source, it demonstrates the high potential of GaSb QDs to be good single photon sources when excited resonantly.

4. Conclusion

We have investigated the characteristics of narrow-linewidth PL-features from GaSb QDs, analyzing time resolved PL and the second order correlation function of a stream of photons from an exciton that are the first measurements of their kind on this material platform.

Exciting above-bandgap, the fine structure splitting of the exciton could be determined to $\Delta E_{FSS} = (12.0 \pm 0.5)$ μeV. Moreover, the time-resolved signature of the exciton recombination photons reveals a slow rise of the PL intensity after excitation. This slow rise points toward the existence of multiple charge injection channels. By solving a system of three coupled differential equations, we have been able to fit the data, extracting the radiative lifetime of the exciton to be $T_1^X = (431 \pm 10)$ ps. The complex filling mechanisms from the QW Γ- and L-valley when exciting above bandgap also reflect in the autocorrelation measurement, where double excitations during one laser pulse could be observed.

Nevertheless, we have been able to prove the non-classical nature of the PL of the investigated charge complex by measuring a $g^{(2)}(0)$ value of 0.16 ± 0.02. A drop of correlated count-events at zero delay time suggests that GaSb QDs have a high potential to be good sources of single photons under resonant pumping.

Supporting Information

Supporting Information is available from the Wiley Online Library or from the author.

Acknowledgements

The University of Wuerzburg group is grateful for financial support by the German Ministry for Research and Education (BMBF) through the project QR.X (FKZ: 16KISQ010) and the State of Bavaria. THL acknowledges funding from the BMBF through the Quantum Futur (FKZ: 13N16272) initiative. The Tampere group acknowledges financial support from the Academy of Finland project QuantSi (decision No 323989) and the Business Finland co-innovation project QuTI.(41739/31/2020).

Open access funding enabled and organized by Projekt DEAL.

Conflict of Interest

The authors declare no conflict of interest.

Data Availability Statement

The data that support the findings of this study are available from the corresponding author upon reasonable request.

Keywords

gallium-antimonide, quantum communication, quantum light sources, semiconductor quantum dots, telecom wavelengths

Received: June 19, 2023
Revised: September 20, 2023
Published online: October 17, 2023

[1] C. Couteau, S. Barz, T. Durt, T. Gerrits, J. Huwer, R. Prevedel, J. Rarity, A. Shields, G. Weihs, *Nat. Rev. Phys.* **2023**, *5*, 326.
[2] A. Gruber, A. Dräbenstedt, C. Tietz, L. Fleury, J. Wrachtrup, C. von Borczyskowski, *Science* **1997**, *276*, 2012.
[3] D. B. Higginbottom, L. Slodicka, G. Araneda, L. Lachman, R. Filip, M. Hennrich, R. Blatt, *New J. Phys.* **2016**, *18*, 093038.
[4] L. Schweickert, K D. Jöns, K D. Zeuner, S. F. Covre Da Silva, H. Huang, T. Lettner, M. Reindl, J. Zichi, R. Trotta, A. Rastelli, V. Zwiller, *Appl. Phys. Lett.* **2018**, *112*, 93106.
[5] P. Michler, A. Imamoglu, A. Kiraz, C. Becher, M. D. Mason, P. J. Carson, G. F. Strouse, S. K. Buratto, W. V. Schoenfeld, P. M. Petroff, *Phys. Staus. Solidi B* **2002**, *229*, 399.
[6] P. Michler, A. Kiraz, C. Becher, W. V. Schoenfeld, P. M. Petroff, L. Zhang, E. Hu, A. Imamoglu, *Science* **2000**, *290*, 2282.
[7] N. Somaschi, V. Giesz, L. De Santis, J. C. Loredo, M. P. Almeida, G. Hornecker, S. L. Portalupi, T. Grange, C. Antón, J. Demory, C. Gómez, I. Sagnes, N. D. Lanzillotti-Kimura, A. Lemaítre, A. Auffeves, A. G. White, L. Lanco, P. Senellart, *Nat. Photonics* **2016**, *10*, 340.
[8] C. Santori, D. Fattal, J. Vuckovic, G S. Solomon, Y. Yamamoto, *Nature* **2002**, *419*, 594.
[9] C. K. Hong, Z. Y. Ou, L. Mandel, *Phys. Rev. Lett.* **1987**, *59*, 2044.
[10] X. Ding, Yu He, Z.-C. Duan, N. Gregersen, M.-C. Chen, S. Unsleber, S. Maier, C. Schneider, M. Kamp, S. Höfling, C.-Y. Lu, J.-W. Pan, *Phys. Rev. Lett.* **2016**, *116*, 20401.
[11] C. H. Bennett, G. Brassard, in *Proceedings of IEEE International Conference on Computers, Systems and Signal Processing, Bangalore, India*, IEEE, Piscataway, NJ, **1984**, pp. 175–179.
[12] S.-K. Liao, W-Qi Cai, W.-Y. Liu, L. Zhang, Y. Li, Ji-G Ren, J. Yin, Qi Shen, Y. Cao, Z.-P. Li, F.-Z. Li, X.-W. Chen, Li-H Sun, J.-J. Jia, J.-C. Wu, X.-J. Jiang, J.-F. Wang, Y.-M. Huang, Q. Wang, Yi-L Zhou, L. Deng, T. Xi, Lu Ma, T. Hu, Q. Zhang, Yu-Ao Chen, N-Le Liu, X.-B. Wang, Z.-C. Zhu, C.-Y. Lu, et al., *Nature* **2017**, *549*, 43.
[13] D. Stucki, N. Walenta, F. Vannel, R. T. Thew, N. Gisin, H. Zbinden, S. Gray, C. R. Towery, S. Ten, *New J. Phys.* **2009**, *11*, 075003.
[14] D. A. Vajner, L. Rickert, T. Gao, K. Kaymazlar, T. Heindel, *Adv. Quantum. Tech.* **2022**, *5*, 2100116.
[15] L. Zhai, G N. Nguyen, C. Spinnler, J. Ritzmann, M C. Löbl, A D. Wieck, A. Ludwig, A. Javadi, R J. Warburton, *Nat. Nanotechnol.* **2022**, *17*, 829.
[16] L. Yu, C M. Natarajan, T. Horikiri, C. Langrock, J S. Pelc, M G. Tanner, E. Abe, S. Maier, C. Schneider, S. Höfling, M. Kamp, R H. Hadfield, M M. Fejer, Y. Yamamoto, *Nat. Commun.* **2015**, *6*, 8955.
[17] X. You, M.-Y. Zheng, Si Chen, R-Ze Liu, J. Qin, Mo-C Xu, Z.-X. Ge, T.-H. Chung, Yu-K Qiao, Y.-F. Jiang, H.-S. Zhong, M.-C. Chen, H. Wang, Yu-M He, X.-P. Xie, H. Li, Li-X You, C. Schneider, J. Yin, T.-Y. Chen, M. Benyoucef, Y.-H. Huo, S. Höfling, Q. Zhang, C.-Y. Lu, J.-W. Pan, *Adv. Photonics* **2022**, *4*, 066003.
[18] M. Anderson, T. Müller, J. Huwer, J. Skiba-Szymanska, A. B. Krysa, R. M. Stevenson, J. Heffernan, D. A. Ritchie, A. J. Shields, *npj Quantum Inf.* **2020**, *6*, 1.
[19] H.-K. Lo, M. Curty, B. Qi, *Phys. Rev. Lett.* **2012**, *108*, 130503.
[20] H.-J. Briegel, W. Dür, J. I. Cirac, P. Zoller, *Phys. Rev. Lett.* **1998**, *81*, 5932.
[21] X. Liu, K. Akahane, N. A. Jahan, N. Kobayashi, M. Sasaki, H. Kumano, I. Suemune, *Appl. Phys. Lett.* **2013**, *103*, 61114.
[22] J. Kaupp, Y. Reum, F. Kohr, J. Michl, Q. Buchinger, A. Wolf, G. Peniakov, T. Huber-Loyola, A. Pfenning, S. Höfling, *Adv. Quantum Technol.* **2023**, *6*, 2300242.
[23] E. S. Semenova, R. Hostein, G. Patriarche, O. Mauguin, L. Largeau, I. Robert-Philip, A. Beveratos, A. Lemaître, *J. Appl. Phys.* **2008**, *103*, 103533.
[24] C. Nawrath, R. Joos, S. Kolatschek, S. Bauer, P. Pruy, F. Hornung, J. Fischer, J. Huang, P. Vijayan, R. Sittig, M. Jetter, S. L. Portalupi, P. Michler, *Adv. Quantum Technol.* **2023**, *6*, 2300111.
[25] M. Paul, F. Olbrich, J. Höschele, S. Schreier, J. Kettler, S. L. Portalupi, M. Jetter, P. Michler, *Appl. Phys. Lett.* **2017**, *111*, 33102.
[26] F. Olbrich, J. Höschele, M. Müller, J. Kettler, S. Luca Portalupi, M. Paul, M. Jetter, P. Michler, *Appl. Phys. Lett.* **2017**, *111*, 133106.
[27] P. Holewa, E. Zięba-Ostój, D. A. Vajner, M. Wasiluk, B. Gaál, A. Sakanas, M. Burakowski, P. Mrowiński, B. Krajnik, M. Xiong, A. Huck, K. Yvind, N. Gregersen, A. Musiał, T. Heindel, M. Syperek, E. Semenova. arXiv:2304.02515, **2023**.
[28] S. Haffouz, K D. Zeuner, D. Dalacu, P J. Poole, J. Lapointe, D. Poitras, K. Mnaymneh, X. Wu, M. Couillard, M. Korkusinski, E. Schöll, K D. Jöns, V. Zwiller, R L. Williams, *Nano Lett.* **2018**, *18*, 3047.
[29] C.-M. Lee, M. A. Buyukkaya, S. Aghaeimeibodi, A. Karasahin, C J. K. Richardson, E. Waks, *Appl. Phys. Lett.* **2019**, *114*, 171101.
[30] T. Gao, L. Rickert, F. Urban, J. Große, N. Srocka, S. Rodt, A. Musial, K. Zolnacz, P. Mergo, K. Dybka, W. Urbanczyk, G. S?K, S. Burger, S. Reitzenstein, T. Heindel, *Appl. Phys. Rev.* **2022**, *9*, 11412.
[31] L. Dusanowski, C. Nawrath, S L. Portalupi, M. Jetter, T. Huber, S. Klembt, P. Michler, S. Höfling, *Nat. Commun.* **2022**, *13*, 748.
[32] A. J. Ramsay, *Semicond. Sci. Technol.* **2010**, *25*, 103001.
[33] R. Stockill, C. Le Gall, C. Matthiesen, L. Huthmacher, E. Clarke, M. Hugues, M. Atatüre, *Nat. Commun.* **2016**, *7*, 12745.
[34] S. F. C. Da Silva, G. Undeutsch, B. Lehner, S. Manna, T M. Krieger, M. Reindl, C. Schimpf, R. Trotta, A. Rastelli, *Appl. Phys. Lett.* **2021**, *119*, 120502.
[35] L. Zaporski, N. Shofer, J H. Bodey, S. Manna, G. Gillard, M. H. Appel, C. Schimpf, S. F. Covre Da Silva, J. Jarman, G. Delamare, G. Park, U. Haeusler, E A. Chekhovich, A. Rastelli, D A. Gangloff, M. Atatüre, C. Le Gall, *Nat. Nanotechnol.* **2023**, *18*, 257.
[36] M. Gurioli, Z. Wang, A. Rastelli, T. Kuroda, S. Sanguinetti, *Nat. Mater.* **2019**, *18*, 799.
[37] Zh. M. Wang, B. L. Liang, K. A. Sablon, G. J. Salamo, *Appl. Phys. Lett.* **2007**, *90*, 113120.
[38] A. Stemmann, Ch. Heyn, T. Köppen, T. Kipp, W. Hansen, *Appl. Phys. Lett.* **2008**, *93*, 123108.
[39] J. Hilska, A. Chellu, T. Hakkarainen, *Cryst. Growth Des.* **2021**, *21*, 1917.
[40] A. Chellu, J. Hilska, J.-P. Penttinen, T. Hakkarainen, *APL Mater.* **2021**, *9*, 51116.
[41] D. Huber, M. Reindl, Y. Huo, H. Huang, J S. Wildmann, O G. Schmidt, A. Rastelli, R. Trotta, *Nat. Commun.* **2017**, *8*, 15506.
[42] M. Bayer, G. Ortner, O. Stern, A. Kuther, A. A. Gorbunov, A. Forchel, P. Hawrylak, S. Fafard, K. Hinzer, T. L. Reinecke, S. N. Walck, J. P. Reithmaier, F. Klopf, F. Schäfer, *Phys. Rev. B* **2002**, *65*, 195315.
[43] L. Leguay, A. Chellu, J. Hilska, E. Luna, A. Schliwa, M. Guina, T. Hakkarainen. arXiv:2308.15418, **2023**.
[44] A. Forchel, U. Cebulla, G. Tränkle, H. Kroemer, S. Subbanna, G. Griffiths, *Surf. Sci.* **1986**, *174*, 143.
[45] D. Smith, E. O'Sullivan, L. Rota, A. Maciel, J. Ryan, *Phys. E* **1998**, *2*, 156.
[46] K. C. Hall, S. W. Leonard, H. M. Van Driel, A. R. Kost, E. Selvig, *Appl. Phys. Lett.* **2000**, *77*, 2882.
[47] A. Mittelstädt, A. Schliwa, P. Klenovský, *Light Sci Appl* **2022**, *11*, 17.
[48] C. P. Chang, Y.-T. Lu, *Solid State Commun.* **1994**, *89*, 949.